Helium implanted gallium nitride evidence of gas-filled rod-shaped cavity formation along the *c*-axis

Jean-François Barbot,[1,a)] Frédéric Pailloux,[1] Marie-Laure David,[1] Laurent Pizzagalli,[1] Erwan Oliviero,[1,2] and Guillaume Lucas[1,3]
[1]*Laboratoire de Physique des Matériaux, UMR 6630 CNRS, Université de Poitiers, SP2MI, Téléport 2, Bd M. & P.Curie, BP30179, 86962 Futuroscope-Chasseneuil Cedex, France*
[2]*Centre de Spectrométrie Nucléaire et de Spectrométrie de Masse, Bât. 108, 91405 Orsay Campus, France*
[3]*Fusion Technology Materials Division, CRPP-EPFL, Villigen-PSI, Suisse 5232, Switzerland*

(Received 11 April 2008; accepted 17 June 2008; published online 28 August 2008)

The structural defects induced by He implantation in GaN epilayer at high fluence (1×10^{17} He/cm^2) and elevated temperature (750 °C) have been studied by conventional and high resolution transmission electron microscopy. In addition to the planar interstitial-type defects lying in the basal plane usually observed after high fluence implantation into GaN, a continuous layer of bubbles arranged in rows parallel to the implanted surface is observed in the region of maximum He concentration. This arrangement of bubbles is ascribed to interactions with dislocations. Beyond, one dimensional rod-shaped defects appear perpendicular to the implanted surface. Contrast analysis of high resolution images and atomistic simulations gives converging results in the determination of the nature and structure of these defects, i.e., gas-filled rod-shaped cavities in an overpressurized state. © *2008 American Institute of Physics*. [DOI: 10.1063/1.2970062]

I. INTRODUCTION

GaN and related group-III nitrites are particularly attractive semiconductors for optoelectronic (laser diodes and UV detectors), microwave power, and ultrahigh power switches applications. Microelectronic GaN devices are grown epitaxially on various substrates such as Si, SiC, and Al_2O_3. The significant thermal expansion and the crystalline structural mismatch between the substrate and the GaN layer induce substantial levels of strain leading to the formation of extended defects such as threading dislocations and nanopipes. These defects have disastrous effects on the optoelectronic and electronic properties of these epilayers. Many studies have thus been devoted to the understanding of their nucleation and to the reduction in their density in the epilayer.[1–3]

Ion implantation is an attractive process for selective area doping of GaN device structures.[4] The effects of ion implantation into GaN have thus been the subject of several reviews.[5,6] The most striking feature of ion implantation into GaN is the formation of planar defects parallel to the basal plane. The implantation of light ions (H, He) is also used for the transfer of thin GaN semiconductor films by means of the Smart Cut™ technology.[7] Thin-film GaN-on-insulator substrates offer new solutions for the microelectronic industry to improve both the performances of the future GaN-based devices and the substrate's mechanical properties.[8] Recently, high fluence He implantation has also been used to form cavities in GaN. The technological interest of forming cavities in GaN is their potential use for the dislocation annihilation.[9] Dislocation inhibition through cavities has been previously reported in He-implanted Si.[10] In the past ten years the formation of nanocavities into semiconductors (Si especially) by He ion implantation and annealing has been extensively studied for their use as sinks for proximity gettering of metallic impurities.[11] Overview of cavity formation and evolution in He-implanted Si have already been published.[12] These cavities have also been found to enhance the strain relaxation and to reduce the threading dislocation density of SiGe/Si heterostructures.[13] Therefore, studies have been carried out varying the conditions of implantation to understand their formation in different semiconductors. In Si, concurrently to cavity formation, interstitial-type defects lying on {113} planes (rodlike and ribbonlike defects) appear in the region of ion's end of range as the implantation temperature is increased.[14] A few degrees of difference in the substrate temperature can also have a significant effect on the density and morphology of cavities, showing the interaction between the implanted He atoms and the radiation damage.[15] In SiC, implantation at elevated temperature avoids the amorphization and small bubbles, lying along rows in the basal plane, are formed in the highly damaged region.[16,17] Rows of bubbles have also been observed in GaAs and ascribed to dislocation formation; the interaction between dislocations and bubbles increases with the temperature.[18] In general, beyond a threshold temperature, no more cavities are formed.[14,17,18] H implantation into GaN results in the formation of H_2 bubbles and after subsequent annealing in faceted voids.[5] Heavy-ion bombardment can lead to the formation of N_2 gas bubbles due to the ion-beam induced stoichiometric imbalance.[5] Recent results on high fluence C ion implantation in GaN showed the formation of large N_2 gas bubbles beyond the maximum of the nuclear deposited energy that was imputed to the stoichiometric imbalance as well.[19] However, many outstanding questions remain regarding the mechanisms of cavity formation in all these semiconductors.

In reference to all these various aspects, understanding

[a)]Author to whom correspondence should be addressed. Electronic mail: jean.francois.barbot@univ-poitiers.fr.

the damage buildup, its recovery as well as the as-created defects are necessary to enhance the performances of the GaN-based devices. This knowledge is also mandatory to develop smart "defect engineering" techniques for GaN as currently done for Si (e.g., shallow junction formation). The purpose of the present work is to study the defects generated by a high fluence He implantation at elevated temperature. Transmission electron microscopy (TEM) experiments and atomistic simulations have been used. Among the techniques suitable for studying the implantation induced damage, TEM is particularly efficient, as it provides a large scale of investigation from several tenths of micrometers to the atomic resolution. High resolution TEM (HRTEM) is also a particularly relevant technique for determining the atomic structure of structural defects. In complement to experiments, it is possible to perform atomistic calculations to compute the atomic structure and the resulting strain field around extended defects. Apart from the physical insight provided by these numerical simulations, calculated atomic coordinates can be used as input parameters in HRTEM image simulation software that constitutes a powerful approach to solve the atomic structure of defect.

II. EXPERIMENTAL DATA AND SETUP

GaN single crystal (7 μm thick) was epitaxially grown on a (0001)-sapphire substrate by metal-organic chemical vapor deposition at 1050 °C. This sample was then implanted with 50 keV He^+ ions using an Eaton implantor at a given current density of 4 $\mu A\,cm^{-2}$. The implantation was performed at 750 °C to study the effect of the implant temperature on defect formation. SRIM 2006 calculations[20] using the displacement energies given by Nord *et al.*[21] predict a mean projected range $R_p=260$ nm and a straggling $\Delta R_p=70$ nm.

The samples were then prepared in cross-section geometry for TEM investigations. The thinning was performed in two steps: Mechanical polishing using a tripod polisher[22] was carried out to reach a thickness of roughly 5 μm and then the final thinning was achieved with a Gatan-PIPS ion miller operated at 2.5 keV (Ar) and grazing incidence ($\pm 6°$) until electron transparency.[23] This method provides wide thin areas that are tricky to obtain as a consequence of the huge internal stress of the GaN epilayer (14% of lattice mismatch). Thin cross sections were then studied using a JEOL 3010 HRTEM (LaB_6, $C_s=1.2$ mm) operating at 300 kV. Fresnel contrast was examined in overfocus and underfocus conditions to determine the nature of defects produced by the implantation process. Focus series were then acquired and compared to images computed with the EMS package[24] in order to analyze the atomic structure of defects. The multislice method was used to take into account the presence of the defects; the thickness of each slice was set to the lattice parameter of bulk GaN ($a_0=0.319$ nm). Prior to these calculations, the multislice method was compared to the Bloch-wave method applied to a perfect crystal in order to validate the simulation parameters [especially the width of the slices of the GaN-wurtzite unit cell viewed along the (11–20) direction] used for the multislice calculations. The Debye–Waller factors were set to 5×10^{-3} nm^2 for both atomic species (the actual values of these factors for atoms located around defects are most probably higher than the ones we have used, but slight variations in this factor would not strongly modify the simulated contrast; it should weakly blur the contrast). The aperture diameter used for the calculations was 14 nm^{-1} and the defocus spread of our microscope was estimated to be 8 nm. Absorption coefficients were set to zero for both atomic species.

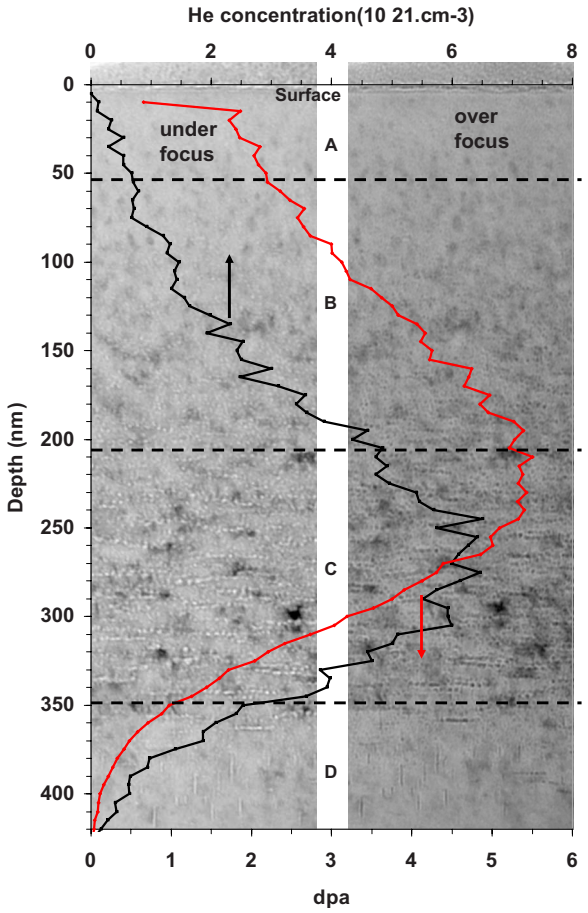

FIG. 1. (Color online) Range and damage distribution for 50 keV He implantation into GaN calculated using SRIM superimposed on bright-field underfocus (bottom) and overfocus (upper) images of the cross section of a GaN sample implanted with 1×10^{17} He/cm^2 at 750 °C. The implanted zone is divided into four regions named A, B, C, and D corresponding to different microstructures.

III. RESULTS

A. General feature of the damaged structure

Figure 1 shows a typical cross-sectional TEM view of the microstructure in GaN implanted at 750 °C with a fluence $\phi=1\times10^{17}$ He/cm^2. As expected, the elevated implantation temperature avoids the amorphization and leads to the formation of a continuous damaged zone around R_p. The damage layer can be divided into four different regions, named A–D, according to the defect density and type. The near surface region, region A, is weakly affected by the implantation process; no particular contrasts are observed whatever the illumination conditions of the sample. Region B, approximately 150 nm wide, begins at about 50 nm beneath the surface where defects become resolvable by conventional

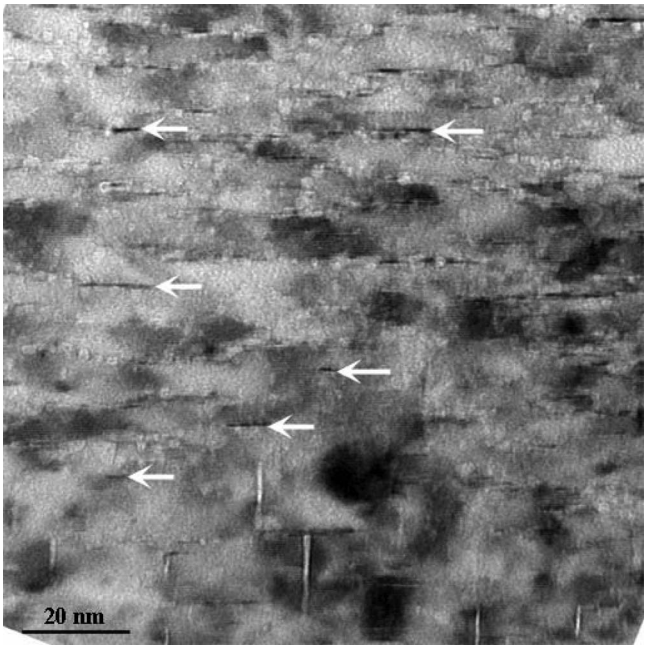

FIG. 2. Magnification of the transition zone between C and D regions, showing the diffraction contrast induced by DLs in the (0001) planes, which appear as dark lines parallel to the surface sample (in this image the surface is horizontal).

TEM. The reversal of the Fresnel contrast between underfocus and overfocus images (Fig. 1) unambiguously proves that these defects are cavities (the Fresnel fringe results from a lowering of the mean inner potential). These tiny cavities (1–2 nm in diameter) are randomly distributed in the layer with a density that increases with increasing depth. Region B ends where cavities appear to lie along rows, i.e., at approximately 200 nm beneath the surface. The striking feature of region C, approximately 150 nm wide, is that the cavities are distributed along chains or rows, lying in the (0001) basal plane of the GaN wurtzite-structure. In this region, the diffraction contrasts also show the presence of structural defects such as dislocations and stacking faults bounded to the spherical cavities. This is clearly highlighted in the HRTEM micrograph (Fig. 2, see the arrows). Vacancy and He concentration depth profiles superimposed on the cross-section TEM image show that this region, C, is centered on the He profile. Deeper in the sample, a fourth region, labeled D, exhibits one dimensional (1D) rod-shaped defects perpendicular to the implanted surface. Their diameter is less than 1 nm (two to three times the in-plane lattice parameter) and their elongation (along the 0001 direction) can reach 10 nm. These defects are located in a relatively narrow band, 50 nm thick. Their contrast behavior under defocusing experiments is similar to that of spherical cavities observed in both regions, B and C (see Fig. 1). These defects have thus been named rod-shaped cavities. Some dislocation loops (DLs) parallel to the basal plane are also observed in this region (their density decreases with increasing depth). Except in the transition zone between regions C and D, no spherical cavities are observed in this deep region.

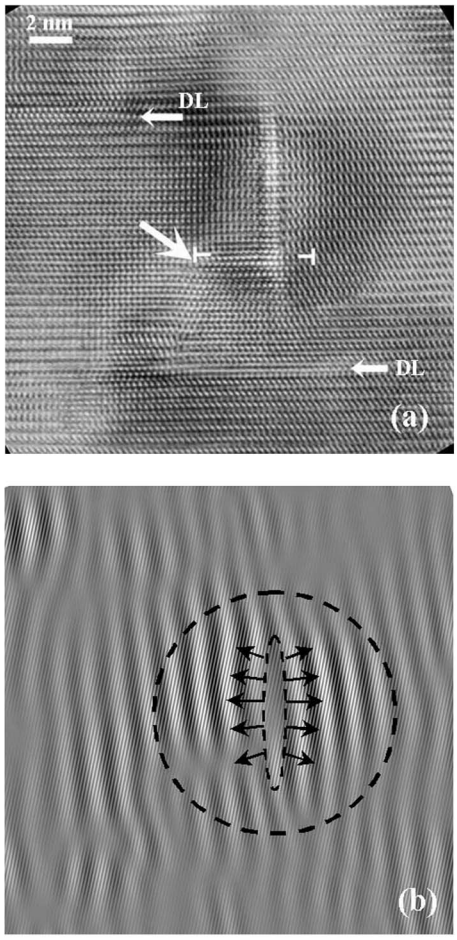

FIG. 3. Cross-sectional TEM micrograph of region D showing a rod-shaped cavity in He-implanted GaN at 750 °C. (a) HRTEM micrograph of the rod-shaped cavity emitting a DL (arrow). Some DLs are also present in the picture. (b) The digital Moiré pattern showing the compressive strain field around the defect (dashed lines have been drawn as guide for eyes).

B. HRTEM observation of the rod-shaped cavities

As stated in Sec. I, the damage accumulation in GaN generally results in the formation of planar defects parallel to the basal plane.[5] The presence of the rod-shaped cavities perpendicular to the implanted surface in the deeper part of the as-damaged zone (Fig. 1) was unexpected and therefore studied in detail. A more systematic HRTEM study has thus been carried out on these particular defects. Figure 3(a) shows the typical contrast surrounding these defects. The origin of this contrast might arise from many different causes. In particular, the local thickness variations due to the sample preparation can strongly affect the high resolution contrast. Thickness-defocus maps have thus been calculated by using the Bloch-wave methods (not shown here) to estimate the magnitude of contrast variation due to thickness inhomogeneities. From these simulations we can deduce that the huge variation in contrast observed experimentally cannot be ascribed to pure thickness differences. It is thus mainly ascribed to the strain induced by the defect itself. This contrast has then been analyzed by means of digital Moiré. It consists of superimposing a perfect reference lattice on a chosen family of planes (selected by Bragg filtering of the fast Fourier transform of the picture). Then the Moiré

pattern magnifies the strain experienced by these planes. This process has been applied to the lattice planes parallel to the defect of Fig. 3(a). The result is depicted in Fig. 3(b); the curvature of the fringes around the defect shows that these rod-shaped defects induce a compressive strain field spreading out up to several tens of nanometers. Despite the fact that it is hardly possible to determine whether this strain field is only due to the defects or to a combination with some relaxation processes during the cross-section thinning, it would suggest that these rod-shaped cavities are overpressurized, i.e., gas filled.

Moreover, as seen in Fig. 3(a), some of these rod-shaped cavities are associated with DLs (see the arrow) in the basal plane. Isolated DLs are also present in the HRTEM micrograph.

C. Atomistic calculation of the rod-shaped cavities

Atomistic calculations have been performed in order to determine the structure of the rod-shaped cavities. The interatomic forces in GaN have been described using a Stillinger–Weber-like semiempirical potential.[25] The latter, fitted on elastic constant lattice parameters of the wurtzite GaN, has been shown to reproduce the dislocation core structures in fair agreement with first-principles calculations,[25] so we expect it is well suited to investigate extended defects in GaN.

Bulk wurtzite GaN has been modeled using a large $20a_0 \times 12\sqrt{2}a_0 \times 25c_0$ (a_0=3.1895 Å, c_0=5.2138 Å) simulation cell, i.e., 48 000 atoms, periodically repeated in space. These dimensions are large enough to cancel spurious defect-defect interactions due to periodicity. Possible structures for a single rod-shaped cavity have been built by removing selected atoms. Those were initially contained in the common volume shared by a cylinder oriented along the 0001 c-axis and an ellipsis centered on the cell. The cylinder allowed obtaining a rod-shaped defect with variable lateral extension while the ellipsis limited the defect length by forming spherical caps at the cylinder extremities. With this procedure, variable sizes of rod-shaped defects, from $2a_0$ to $4a_0$ in diameter and from $11c_0$ to $13c_0$ in length, were obtained and relaxed in our simulations. Starting from an initial defect configuration, the system's total energy has been minimized until all interatomic forces become lower than 10^{-5} eV Å^{-1}. It has to be noted that the same number of Ga and N atoms has been removed to form the cavities; thus, keeping the electronic neutrality of the system.

Figure 4 shows one defect and its relaxed lateral structure. As a result of the building procedure, the inner surface of the cavities is nonpolar since it includes an equal number of Ga and N atoms. One bond per atom is suppressed, leaving Ga–N dimers with a bond length equal to the first-neighbor bulk distance and oriented along 0001. This surface structure is very stable and is not modified by force relaxation. As a result, there is almost no relaxation energy associated with the lateral surface. The larger atomic displacements have been found to be localized in both ends of the rod-shaped cavities. They remain relatively small, however, and further investigation of the Von Mises stress distribution in the vicinity of the defect reveals a very small perturbation

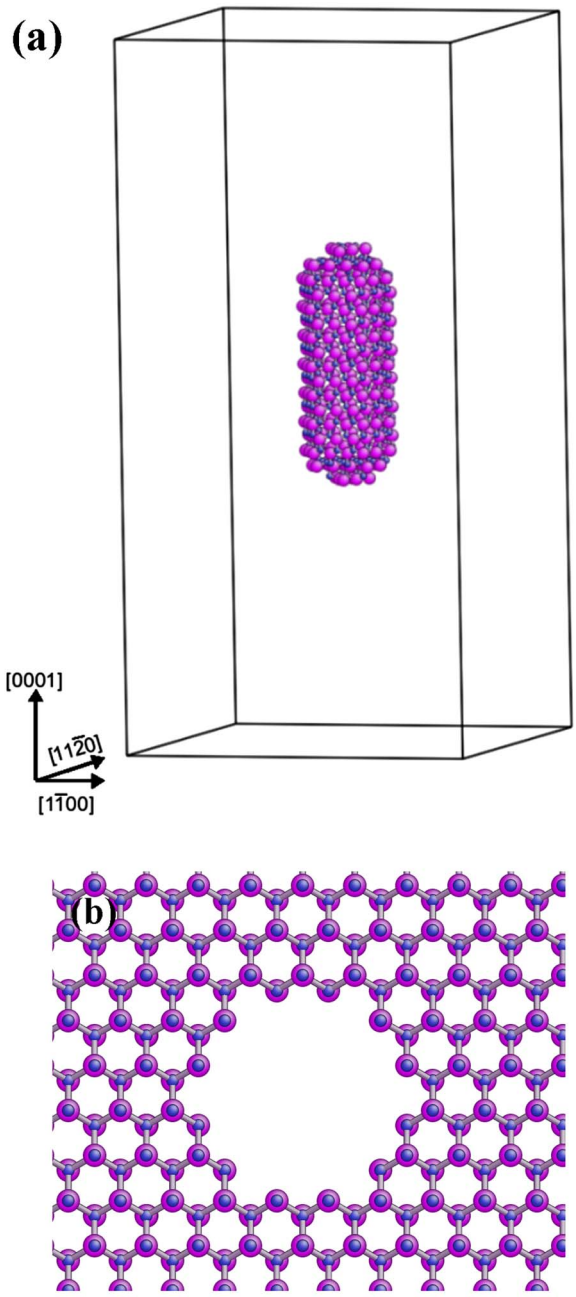

FIG. 4. (Color online) Ball-and-stick representations of one cavity, with N atoms as small blue spheres and Ga atoms as big magenta spheres. (a) Simulation cell with one cavity in the center. Only atoms in the vicinity of the cavity are shown for clarity. (b) Slice along the 0001 direction showing the inner surface of one relaxed cavity ($4a_0$ width).

of the embedding lattice. Varying the defect dimension did not qualitatively change these results. Relaxed inner surface geometries can be compared with previous works on GaN flat surfaces. First-principles calculations predicted a small buckling of Ga–N dimers on 10–10 and 11–20 surfaces,[26,27] in disagreement with our flat bulklike dimers. This buckled surface reconstruction results from an electronic structure rearrangement due to a charge transfer between Ga and N, and cannot be described by the semiempirical Stillinger–Weber potential used in our calculations. However, it is unlikely that the small atomic displacements due to the buckling would

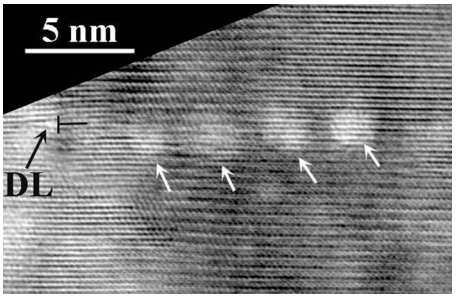

FIG. 5. HRTEM micrograph of the bottom part of region C showing one chaplet of cavities (arrows) lying along the edge of the DLs.

induce a large compressive strain several nanometers away from the surface of the defect. This also promotes the idea that these cavities are gas filled as suggested by the HRTEM analysis (see the previous section).

IV. DISCUSSION

At high fluence and elevated temperature, He implantation in GaN produces a multilayer damaged structure containing different types of extended defects. In the near surface region A, due to the low He concentration, any He-vacancy clusters can be formed so that vacancies undergo annihilation presumably by migrating to the surface of the epilayer (the migrating energy of the Ga vacancy $E_m^{V_{Ga}} \approx 1.5$ eV).[28] He is also supposed to be mobile at this temperature and can desorb from the matrix when not trapped by vacancies. Therefore, no cavities are formed in the first tens of nanometers of the GaN epilayer. In region B, an isolated cavity system is formed due to the relatively low concentration of mobile He with a pretty high concentration of damage. The vacancy-type defects are stabilized when trapping mobile He forming thus cavities during the implantation. Even if the details of the processes are not known, the cavity formation does not seem to differ from other semiconductors.[11] The system, dislocation-cavity rows, observed in region C has also been reported in other He-implanted semiconductors (SiC implanted at 750 °C and GaAs implanted at temperature up to 150 °C).[17,18] Figure 5 clearly shows that the cavities are attached to dislocations. The formation of DLs in the basal plane results from the agglomeration of interstitials. The presence of DLs beyond the cavity layer comes from the spatial separation of Frenkel pairs; the interstitial having a deeper distribution profile.[29,30] Planar defects lying in the basal plane are characteristic of GaN bombarded with ions under a wide range of implantation conditions.[5] A similar mechanism is observed in implanted Si at elevated temperature where {311} defects are observed beyond the bubble layer.[14,31] These DLs could also result from the loop punching phenomenon. In this case, gas-filled cavities (referenced as bubbles) in an overpressurized state can relieve their increasing pressure when the He accumulates during implantation, by punching out interstitial loops. In the latter case the DL density should be higher in the dense layer of cavities, region C, than in region D.

Bubbles are readily formed into GaN when H is implanted at room temperature and subsequently annealed. Upon annealing at temperature above 800 °C, H outgases from the matrix and faceting of the cavities appear.[32] These cavities form polyhedrons with apexes always pointed toward the substrate. Similar cavities, referred as nanovoids, have also been observed after He implantation followed by a rapid thermal annealing into GaN.[8] Polyhedrons are also observed after a prolonged electron irradiation of as-grown nanopipes.[33] These morphologic evolutions are explained by the surface energy minimization. All the cavities formed by the He implantation at 750 °C in GaN are spherical and of small diameter showing that the growth of cavities is limited at this temperature. This is different from what is observed in Si for implantation temperatures higher than 400 °C where growth and faceting of cavities occur at the same time as He is released.[34] He is thus supposed to be retained up to high temperatures in GaN suggesting that the spherical cavities observed in regions B and C are He-filled cavities, i.e., bubbles. This is in agreement with recent results on Ne-implanted Si, which suggest that the presence of Ne in bubbles slows down both the growth and the faceting of bubbles.[31] The role of the impurities is, however, not clear; oxygen, for example, can impede the faceting of the He bubbles in Si (Ref. 35) whereas it is invoked in the formation of pyramidal voids[3] during the GaN growth. More work is needed to confirm the presence of He in the cavities.

The microstructure observed in region D is more puzzling. The reversal of the Fresnel contrast of the 1D rod-shaped defects shows that they are composed of an element or a combination of elements having a potential lower than GaN. From this we can infer that the defect is of vacancy-type and can be named rod-shaped cavities. The contrast analysis suggests that these rod-shaped cavities are gas filled in an overpressurized state. Concurrently, the atomistic calculations show that an empty rod-shaped cavity can only induce a very small perturbation of the embedding lattice. To confirm this last point, atomic positions extracted from the atomistic calculations have been used to perform HRTEM image simulations. Focus series have been calculated for defocus values close to the Scherzer defocus of our microscope ($\Delta F = -57$ nm). The agreement between simulated images and experimental micrograph at the position of the defect is relatively poor. Nevertheless, the contrast variations with defocus values are of same order (Fig. 6). It is also obvious that the strain field observed in the experimental micrographs is not reproduced by the simulations. The rod-shaped defects are thus elongated cylindrical gas-filled cavities in an overpressurized state. If the internal cavity pressure exceeds the pressure required for loop punching, DLs are formed in the basal plane, which could explain why a DL binds the rod-shaped cavity as seen in Fig. 3. This comment also suggests that these cavities are gas filled.

The implantation induces a dilatation gradient normal to the surface. In Si, this in-plane stress favors the formation of H platelets parallel to the as-implanted surface.[36] Recent wafer bowing measurements on high fluence H-implanted GaN gave values of the in-plane compressive stress of a few gigapascals in the damaged layer.[37] In GaN implanted at 750 °C, the abrupt transition of the bubble density between region C (dislocation-bubble lines) and region D (free of isolated bubbles) shows that dislocations are preferential

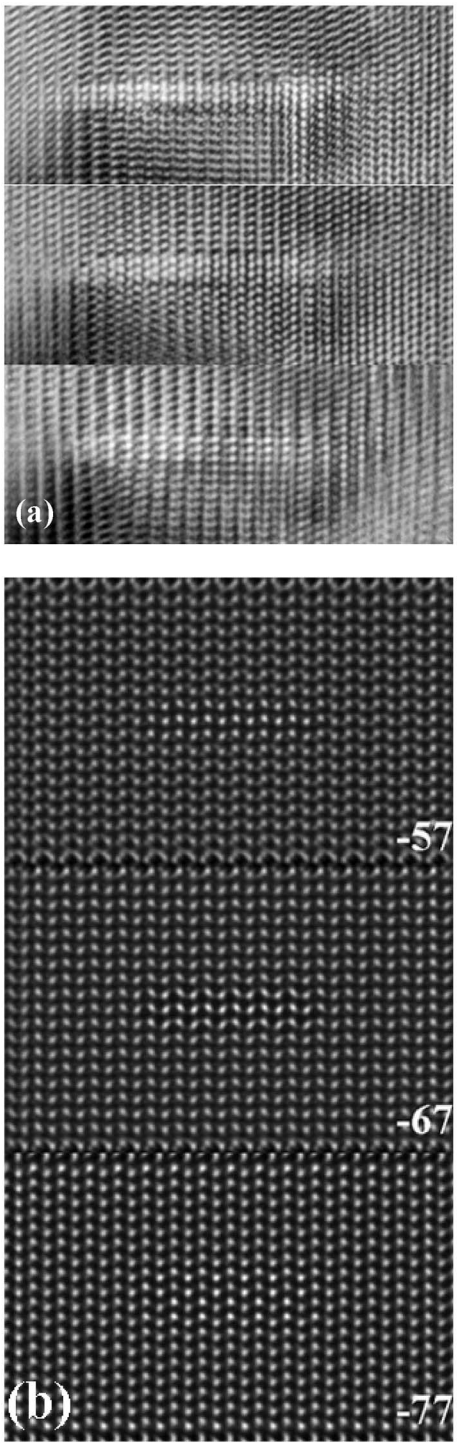

FIG. 6. (a) Experimental focus series of the rod-shaped cavity imaged in Fig. 3 and (b) calculated focus series of an empty cylindrical void. The defocus value is indicated in nanometer in the bottom right corner.

nucleation sites for bubble formation; the out-of-plane strain providing natural space for bubble nucleation. The rod-shaped cavities are only observed in a region, D, where a small strain is expected. In this region where the vacancy concentration is rather low in comparison with the He concentration, another mechanism of defect formation is operating. The formation of these rod-shaped cavities along the *c*-axis is obscure and more work is necessary to propose a mechanism. For example, the presence of impurities has not been taken into account. The oxygen impurities can stabilize Ga vacancies by forming $V_{Ga}-(O_N)_3$ complexes.[38] Such defects are invoked in the formation and overgrowth of nanopipes along the *c*-axis. So, we can easily imagine that they are formed during ion implantation where numerous Ga vacancies are created. These complexes will act as primary sinks for vacancy and by further agglomeration will lead to the formation of nanosized nanopipes. These nanopipes might be able to trap the mobile He.

V. CONCLUSION

The damage structure in GaN film implanted under elevated temperature with high He ion fluence was examined by means of conventional and HRTEM. Spherical bubbles of nanometer size and DLs lying in the basal planes are readily formed during the implantation. A high density of bubbles bounded to DLs is formed in the region of maximum He concentration. Beyond the bubble layer, among the planar defects, rod-shaped cavities are formed along the *c*-axis. Both the contrast analysis and the atomistic calculations infer for gas-filled cavities in an overpressurized state.

[1] J. L. Rouviere, M. Arlery, B. Daudin, G. Feuillet, and O. Briot, Mater. Sci. Eng., B **50**, 61 (1997).
[2] Z. Liliental-Weber, J. Jasinski, and J. Washburn, J. Cryst. Growth **246**, 259 (2002).
[3] D. Cherns and M. E. Hawkridge, Philos. Mag. **86**, 4747 (2006).
[4] S. J. Pearton, J. C. Zolper, R. J. Shul, and F. Ren, J. Appl. Phys. **86**, 1 (1999).
[5] S. O. Kucheyev, J. S. Williams, and S. J. Pearton, Mater. Sci. Eng., R. **33**, 51 (2001).
[6] C. Ronning, E. P. Carlson, and R. F. David, Phys. Rep. **351**, 349 (2001).
[7] A. Tauzin, T Akatsu, M. Rabarot, J. Dechamp, M. Zussy, H. Moriceau, J. F. Michaud, A. M. Charvet, L. Di Cioccio, F. Fournel, J. Garrione, B. Faure, F. Letertre, and N. Kernevez, Electron. Lett. **41**, 668 (2005).
[8] D. Cummings, III-Vs Review **18**, 28 (2005).
[9] D. Alquier, C. Bongiorno, F. Roccaforte, and V. Raineri, Appl. Phys. Lett. **86**, 211911 (2005).
[10] V. Raineri and S. U. Campisano, Appl. Phys. Lett. **69**, 1783 (1996).
[11] D. M. Follstaedt, S. M. Myers, G. A. Petersen, and J. W. Medernach, J. Electron. Mater. **25**, 157 (1996).
[12] V. Raineri, M. Saggio, and E. Rimini, J. Mater. Res. **15**, 1449 (2000).
[13] B. Hollander, S. T. Lenk, S. Mantl, H. Trinkaus, D. Kirch, M. Luysberg, T. Hakbarth, H. J. Herzog, and P. F. P. Fichtner, Nucl. Instrum. Methods Phys. Res. B **175–177**, 357 (2001).
[14] M. L. David, M. F. Beaufort, and J. F. Barbot, J. Appl. Phys. **93**, 1438 (2003).
[15] V. Raineri and M. Saggio, Appl. Phys. Lett. **71**, 1673 (1997).
[16] E. Oliviero, M. L. David, M. F. Beaufort, J. Nomgaudyte, L. Pranevicius, A. Declémy, and J. F. Barbot, J. Appl. Phys. **91**, 1179 (2002).
[17] E. Oliviero, C. Tromas, F. Pailloux, A. Declemy, M. F. Beaufort, C. Blanchard, and J. F. Barbot, Mater. Sci. Eng., B **102**, 289 (2003).
[18] D. M. Follstaedt, S. M. Mayer, J. C. Barbour, G. A. Petersen, J. L. Reno, L. R. Dawson, and S. R. Lee, Nucl. Instrum. Methods Phys. Res. B **160**, 476 (2000).
[19] S. O. Kucheyev, J. E. Bradby, C. P. Li, S. Ruffell, T. van Buuren, and T. E. Felter, Appl. Phys. Lett. **91**, 261905 (2007).
[20] J. F. Ziegler and J. B. Biersack (http://www.srim.org).
[21] J. Nord, K. Nordlund, and J. Keinonen, Phys. Rev. B **68**, 184104 (2003).
[22] J. Ayache and P. H. Albarède, Ultramicroscopy **60**, 195 (1995).
[23] F. Pailloux, D. Imhoff, T. Sikora, A. Barthélémy, J.-L. Maurice, J.-P. Contour, C. Colliex, and A. Fert, Phys. Rev. B **66**, 014417 (2002).
[24] P. A. Stadelmann, Ultramicroscopy **21**, 131 (1987).
[25] A. Béré and A. Serra, Phys. Rev. B **65**, 205323 (2002).
[26] D. Segev and C. Van de Walle, Surf. Sci. **601**, L15 (2007).

[27]J. E. Northrup and J. Neugebauer, Phys. Rev. B **53**, R10477 (1996).
[28]K. Saarinen, T. Suski, I. Grzegory, and D. C. look, Phys. Rev. B **64**, 233201 (2001).
[29]O. W. Holland, J. D. Budai, and B. Nielsen, Mater. Sci. Eng., A **253**, 240 (1998).
[30]P. Pellegrino, P. Levêque, J. Wong-Leung, C. Jagadish, and B. G. Svensson, Appl. Phys. Lett. **78**, 3442 (2001).
[31]E. Oliviero, S. Peripolli, L. Amaral, P. F. P. Fichtner, M. F. Beaufort, J. F. Barbot, and S. Donnelly, J. Appl. Phys. **100**, 043505 (2006).
[32]S. M. Myers, T. J. Headley, C. R. Hills, J. Han, G. A. Petersen, C. H. Seager and W. R. Wampler, MRS Internet J. Nitride Semicond. Res., **4S1**, G5.8 (1999).
[33]F. Pailloux, J. Colin, J. F. Barbot, and J. Grilhé, Appl. Phys. Lett. **86**, 131908 (2005).
[34]E. Oliviero, M. L. David, M. F. Beaufort, J. J. Barbot, and T. van Veen, Appl. Phys. Lett. **81**, 4201 (2002).
[35]V. M. Vishnyakov, S. E. Donnelly, and G. Carter, J. Appl. Phys. **94**, 238 (2003).
[36]M. Nastasi, T. Höchbauer, J. K. Lee, J. P. Hirth, M. Ridgway, and T. Lafford, Appl. Phys. Lett. **86**, 154102 (2005).
[37]R. Singh, I. Radu, G. Bruederl, V. Haerle, U. Gösele, and S. H. Christiansen, Semicond. Sci. Technol. **22**, 418 (2007).
[38]J. Elsner, R. Jones, M. Haugk, R. Gutierrez, Th. Frauenheim, M. I. Heggie, S. Öberg, and P. R. Briddon, Appl. Phys. Lett. **73**, 3530 (1998).